CHARACTERISTICS AND EVOLUTION OF THE MAGNETIC FIELD AND CHROMOSPHERIC EMISSION IN AN ACTIVE REGION CORE OBSERVED BY *HINODE*

David H. Brooks [1,2,3], Harry P. Warren [1], Amy R. Winebarger [4]

dhbrooks@ssd5.nrl.navy.mil

ABSTRACT

We describe the characteristics and evolution of the magnetic field and chromospheric emission in an active region core observed by the Solar Optical Telescope (SOT) on *Hinode*. Consistent with previous studies, we find that the moss is unipolar, the spatial distribution of magnetic flux evolves slowly, and that the magnetic field is only moderately inclined. We also show that the field line inclination and horizontal component are coherent, and that the magnetic field is mostly sheared in the inter-moss regions where the highest magnetic flux variability is seen. Using extrapolations from Spectropolarimeter (SP) magnetograms we show that the magnetic connectivity in the moss is different than in the quiet Sun because most of the magnetic field extends to significant coronal heights. The magnetic flux, field vector, and chromospheric emission in the moss also appear highly dynamic, but actually show only small scale variations in *magnitude* on time-scales longer than the cooling times for hydrodynamic loops computed from our extrapolations, suggesting high-frequency (continuous) heating events. Some evidence is found for flux (Ca II intensity) changes on the order of 100–200 G (DN) on time-scales of 20–30 mins that could be taken as indicative of low-frequency heating. We find, however, that only a small fraction (10%) of our simulated loops would be expected to cool on these time-scales, and we do not find clear evidence that the flux changes consistently produce intensity changes in the chromosphere. Using observations from the EUV Imaging Spectrometer (EIS) we also determine that the filling factor in the moss is $\sim 16\%$, consistent with previous studies and larger than the size of an SOT pixel. The magnetic flux and chromospheric intensity in most individual SOT pixels in the moss vary by less than $\sim 20\%$ and $\sim 10\%$, respectively, on loop cooling time-scales. In view of the high energy requirements of the chromosphere, we suggest that these variations could be sufficient for the heating of 'warm' EUV loops, but that the high basal levels may be more important for powering the hot core loops rooted in the moss. The magnetic field and chromospheric emission appear to evolve gradually on spatial scales comparable to the cross-field scale of the fundamental coronal structures inferred from EIS measurements.

Subject headings: Sun: activity— Sun: magnetic topology—Sun: photosphere—Sun: chromosphere—Sun: corona

1. INTRODUCTION

Significant progress in solving the decades old coronal heating problem could be made if one knew the duration and frequency of heating events. Analysis of soft X-ray loops in the *Yohkoh* era suggested that high temperature (3–5MK) coronal plasma could be heated steadily (Porter & Klimchuk 1995; Kano & Tsuneta 1996). These loops are rooted in the "moss," which is found in active region cores (Martens et al. 2000), and it has been argued that the lack of intensity variations there is indicative of steady heating (Antiochos et al. 2003). Furthermore, hydrostatic modeling of whole active regions has been quite successful at reproducing the core emission from short hot loops (Schrijver et al. 2004; Warren & Winebarger 2006; Lundquist et al. 2008).

Hydrostatic modeling, however, has greater difficulty reproducing the emission at lower temperatures. Warm (1MK) EUV loops observed by the Solar and Heliospheric Observatory (*SOHO*, Domingo et al. 1995) and the Transition Region and Coronal Explorer (*TRACE*, Handy et al. 1999) have been found to be overdense compared to static equilibrium theory and persist far longer than expected loop cooling times (Lenz et al. 1999; Aschwanden et al. 2001; Winebarger et al. 2003). These obser-

vational features can be explained if coronal loops are bundles of unresolved threads that are heated impulsively (Aschwanden et al. 2000; Warren et al. 2002; Winebarger et al. 2003).

Of course, most of the proposed coronal heating mechanisms are impulsive in nature (Klimchuk 2006), and the term 'steady heating' is usually taken to mean that the repetition time between impulsive heating events is shorter than the time it takes for the loop to cool by conduction and then radiation. Loops are thus maintained at high temperatures and the emission is apparently steady. Many active regions appear to evolve slowly and loops are not often seen cooling in the core around the moss in these regions (Antiochos et al. 2003; Patsourakos & Klimchuk 2008). In other cases, loops are clearly seen evolving and cooling (Ugarte-Urra et al. 2009), and it is not clear which type of heating is dominant. Still, it would be surprising if the structure and heating characteristics of warm loops and hot loops were fundamentally different. A challenge to current loop modeling is to draw these pictures together and understand how they can exhibit these apparently contradictory properties.

The instruments on board the *Hinode* satellite (Kosugi et al. 2007) are providing unprecedented observations of active regions in terms of temperature coverage, spatial, temporal, and spectral resolution. As such they are allowing us to probe the properties of moss at the bases of high temperature loops in active region cores in new detail. In two previous papers (Brooks & Warren 2009; Warren et al. 2010, hereafter Paper 1 and Paper 2), we analyzed EUV Imaging Spectrometer (EIS) and X-ray Telescope (XRT) observations of an active region observed by *Hinode* in June 2007 (NOAA 10960) in order to study the time-scale of

[1] Space Science Division, Code 7673, Naval Research Laboratory, Washington, DC 20375

[2] George Mason University, 4400 University Drive, Fairfax, VA 22020

[3] Present address: Hinode Team, ISAS/JAXA, 3-1-1 Yoshinodai, Sagamihara, Kanagawa 229-8510, Japan

[4] Department of Physics, Alabama A&M, 4900 Meridian Street, Normal, AL 35762

Report Documentation Page		

1. REPORT DATE **JUN 2010**	2. REPORT TYPE	3. DATES COVERED **00-00-2010 to 00-00-2010**
4. TITLE AND SUBTITLE **Characteristics and Evolution of the Magnetic Field and Chromospheric Emission in an Active Region Core Observed by Hinode**		5a. CONTRACT NUMBER
		5b. GRANT NUMBER
		5c. PROGRAM ELEMENT NUMBER
6. AUTHOR(S)		5d. PROJECT NUMBER
		5e. TASK NUMBER
		5f. WORK UNIT NUMBER
7. PERFORMING ORGANIZATION NAME(S) AND ADDRESS(ES) **Naval Research Laboratory,Space Science Division,Code 7673,Washington,DC,20375**		8. PERFORMING ORGANIZATION REPORT NUMBER
9. SPONSORING/MONITORING AGENCY NAME(S) AND ADDRESS(ES)		10. SPONSOR/MONITOR'S ACRONYM(S)
		11. SPONSOR/MONITOR'S REPORT NUMBER(S)

12. DISTRIBUTION/AVAILABILITY STATEMENT
Approved for public release; distribution unlimited

13. SUPPLEMENTARY NOTES

14. ABSTRACT

We describe the characteristics and evolution of the magnetic field and chromospheric emission in an active region core observed by the Solar Optical Telescope (SOT) on Hinode. Consistent with previous studies, we find that the moss is unipolar, the spatial distribution of magnetic flux evolves slowly, and that the magnetic field is only moderately inclined. We also show that the field line inclination and horizontal component are coherent, and that the magnetic field is mostly sheared in the inter-moss regions where the highest magnetic flux variability is seen. Using extrapolations from Spectropolarimeter (SP) magnetograms we show that the magnetic connectivity in the moss is different than in the quiet Sun because most of the magnetic field extends to significant coronal heights. The magnetic flux, field vector, and chromospheric emission in the moss also appear highly dynamic, but actually show only small scale variations in magnitude on time-scales longer than the cooling times for hydrodynamic loops computed from our extrapolations, suggesting high- frequency (continuous) heating events. Some evidence is found for flux (Ca ii intensity) changes on the order of 100?200 G (DN) on time-scales of 20?30 mins that could be taken as indicative of low-frequency heating. We find, however, that only a small fraction (10%) of our simulated loops would be expected to cool on these time-scales, and we do not find clear evidence that the flux changes consistently produce intensity changes in the chromosphere. Using observations from the EUV Imaging Spectrometer (EIS) we also determine that the filling factor in the moss is   16%, consistent with previous studies and larger than the size of an SOT pixel. The magnetic flux and chromospheric intensity in most individual SOT pixels in the moss vary by less than   20% and 10%, respectively, on loop cooling time-scales. In view of the high energy requirements of the chromosphere, we suggest that these variations could be sufficient for the heating of ?warm? EUV loops, but that the high basal levels may be more important for powering the hot core loops rooted in the moss. The magnetic field and chromospheric emission appear to evolve gradually on spatial scales comparable to the cross-field scale of the fundamental coronal structures inferred from EIS measurements.

15. SUBJECT TERMS					
16. SECURITY CLASSIFICATION OF:			17. LIMITATION OF ABSTRACT	18. NUMBER OF PAGES	19a. NAME OF RESPONSIBLE PERSON
a. REPORT **unclassified**	b. ABSTRACT **unclassified**	c. THIS PAGE **unclassified**	**Same as Report (SAR)**	**16**	

energy release. Several lines of evidence led to the conclusion that the heating in the core of this region was effectively steady. First, soft X-ray and Fe XII 195.119 Å intensities in the moss were shown to vary by less than 15% over many hours. Second, from the Fe XII 195.119 Å line profiles, we measured Doppler and non-thermal velocities in the moss of ~ 3 km s^{-1} and ~ 26 km s^{-1} on average, respectively. Taking into consideration the uncertainties, and also the fact that Fe XII lines have been shown to be blue-shifted by a few km s^{-1} in the quiet Sun (Peter & Judge 1999), the moss velocity measurement is consistent with zero. In addition, based on a comparison with several quiet Sun synoptic datasets, the measurement of the non-thermal velocity in the moss was shown to be no larger than the typical quiet Sun value of 25 km s^{-1}. More importantly, neither quantity varied by more than 15% over many hours. Third, no evidence was found for co-spatial warm and hot emission, as would be expected from impulsive heating models that assume coronal loops have time to cool substantially between events. Finally, the observed moss intensities could be brought into agreement with hydrostatic simulations provided that local expansion of the magnetic field at the base of the corona was included in the numerical model.

These results rule out the possibility of low frequency impulsive heating of monolithic loops on the spatial scales resolved in the analysis. An alternative possibility, however, is that the heating is impulsive at low frequency on sub-resolution threads, as is thought to be the case in the warm overdense loops (Jim Klimchuk 2009, private communication). This picture may appear like high frequency heating in the observational analysis of Paper 1.

It is clear that we can already resolve the expected loop cooling times temporally, and even other transient activity on localized scales, e.g. short duration "Type II" spicules (de Pontieu et al. 2007) and blinkers (Brooks et al. 2004). Some recent observations by EIS have also suggested that we may be close to resolving the cross field spatial scale of the fundamental coronal structures: see e.g. Warren et al. 2008a who derive loop filling factors of $\sim 10\%$, or Tripathi et al. (2009) who obtained values larger than this except near the base of the loop they analyzed. This also sets an upper limit on the spatial scale of coronal heating in loops, whether the fundamental structures are monolithic or composed of multiple threads. It does not mean, however, that the individual threads of the bundle are resolved. Based on magnetic flux arguments, Priest et al. (2002) suggest that single *TRACE* loops may be composed of 10 or more individual strands, and that the spatial scale we need to observe may be finer still. This is the case for nanoflare heating (Parker 1988) where the reconnection takes place at the current sheets between threads (Klimchuk 2006). Current EUV and X-ray instrumentation are unable to resolve such structure, but the spatial resolution, excellent seeing, and stability of the *Hinode* Solar Optical Telescope (SOT) allow it to observe at much higher spatial resolution than EIS or XRT. A direct comparison between chromospheric and coronal observations is of course difficult because of the large difference in instrumental spatial resolutions, and a lack of knowledge of the influence of the expansion of the field. Therefore, in this paper, we analyze only SOT observations of the magnetic field and chromospheric emission. We again study the core of the June 2007 region analyzed in Paper 1 and Paper 2. Since the observations are new in themselves, we describe the magnetic field characteristics of the moss and active region

core. Our main goal, however, is to study the variation of the magnetic flux, vector field, and chromospheric emission to try to uncover any behavior that could be related to the heating process and would allow us to set further constraints on the heating time-scale in this region.

In §2 we describe the observations and data reduction procedures. In §3 we discuss the magnetic characteristics of the region and in §4 we introduce the modeling that we use to compare the time-scales of observational variability with typical loop cooling times. This is important because it is the crucial time-scale that differentiates between low and high frequency (effectively steady) impulsive heating. We thus put several statements about the evolution of the magnetic field on a quantitative basis. In §5 we examine the variability and evolution of the magnetic field and the chromospheric emission, and find that most of the activity takes place on time-scales longer than the computed theoretical loop cooling times. We also discuss departures from this picture. In §6 we discuss the spatial resolution issue once again and we derive the filling factor for the moss using EIS observations. The results suggest that SOT *may* be able to resolve the cross-field spatial scale of structures in the moss in individual pixels, so we further examine the magnetic flux and chromospheric variability on these size scales §7. The conclusions are presented and discussed in §8.

2. *Hinode* AND *TRACE* OBSERVATIONS

AR 10960 crossed the solar disk between 2007, May 30 and June 14. The region produced numerous C- and M- class flares during that period and was therefore the main observing target for most solar instrumentation on the ground and in space. In this paper we mostly use SOT data, but we also coalign and use *TRACE* 171 Å filter images to identify the coronal features in the active region core, particularly the moss. An XRT Open/Ti-Poly image is also used for giving an overview of the hot core emission, and later we also use EIS data to determine the moss filling factor.

The SOT is described in detail by Tsuneta et al. (2008). It consists of an optical telescope assembly (OTA, Suematsu et al. 2008) that feeds a Filtergraph (FG) instrument and Spectropolarimeter (SP). The FG itself consists of a Broadband Filter Imager (BFI) and a tunable Lyot-type Narrowband Filter Imager (NFI). The NFI can obtain filtergrams, dopplergrams, and Stokes I, Q, U, and V images in a number of spectral lines formed in the solar photosphere and chromosphere. The SP instrument obtains high-precision polarimetric scans in the Fe I 6301 Å and 6302 Å spectral lines. The precision of the polarimetric calibration is discussed in Ichimoto et al. (2008). As it is flown in space and has its own correlation tracker, SOT obtains high quality seeing-free and stable longitudinal or transverse magnetograms that can be used to diagnose magnetic field dynamics in the lower atmosphere.

In this paper we analyze both FG and SP data. Large FOV SP observations are used in §3 to describe the magnetic characteristics of AR 10960. These data were obtained from the SOT level-2 archive. As such they are outputs from the Milne-Eddington gRid Linear Inversion Network (MERLIN) code developed at the Community Spectro-polarimetric Analysis Center (CSAC) at the High Altitude Observatory (HAO) by Bruce Lites and colleagues (Lites et al. 2007). MERLIN performs Levenberg-Marquardt least squares fitting of the full Stokes profiles obtained by the
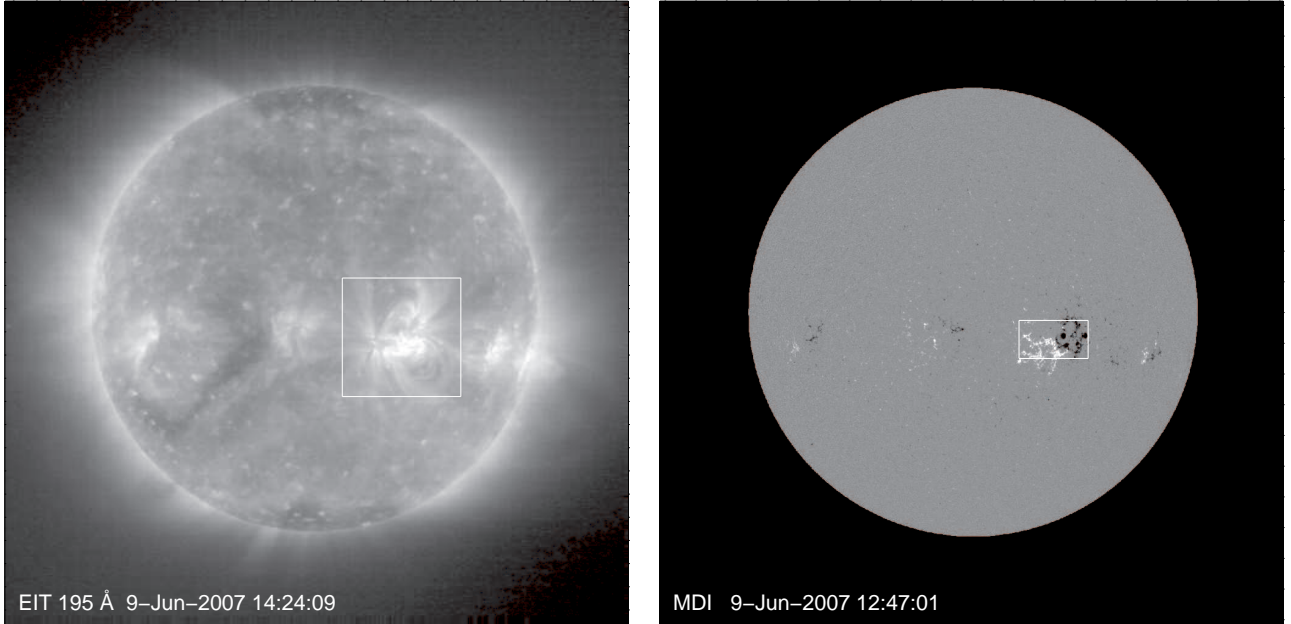
Fig. 1.— Full Sun context images of AR 10960. Left Panel: *SOHO*/EIT 195 Å image with the *TRACE* FOV overlaid as a box. Right Panel: *SOHO*/MDI magnetogram with the *Hinode* SOT FOV overlaid as a box.

SP. Several assumptions about the atmospheric approximation and fit parameter initialization are made, for example, the source function is assumed to be linear with optical depth and the atmosphere is assumed to be in local thermal equilibrium. The level-2 archive data are the parameters that give the best fit to the observed profile and much more detail is given on the level-2 archive website. A key point of note is that no attempt is made to resolve the 180° azimuth ambiguity. This is discussed at the appropriate times below.

The large FOV SP observations we analyze were obtained by scanning the slit over an area of $279.1'' \times 163.8''$ between 14:20:05 and 15:23:17UT on June 09. The resolution of this scan is $0.30'' \times 0.32''$ per pixel and the time for individual polarimetric exposures was 1.6s. Exposures were obtained at each new scan position every 3.8s. In §5 we analyze a time-series of high cadence SP scans obtained between 21:56:03 and 22:59:31UT on June 08. The observing parameters were the same for this run, but the FOV was only $7'' \times 512''$ so the time for each small scan is 28s. These data were also obtained from the level-2 archive.

We also analyze a time-series of FG longitudinal magnetograms obtained in the Na I D 5896 Å line at $\sim$ 30s cadence. The spatial sampling of the Na I D Stokes images was $0.16''$/pixels over a $327.7'' \times 163.8''$ FOV with an effective exposure time of 14.2s created from polarimetric images with individual exposure times of 0.12s. The time-series ran between 18:14:32 and 23:37:04UT on June 09, and the data were processed using the *SolarSoft* routine FG_PREP. The SOT observations were set to complement each other, with similar FOV scans with the SP and FG interspersed with high cadence time-series. They cover approximately 26 hr in total.

To study the variability of chromospheric emission we also analyze a co-temporal FG time-series of Ca II 3896 Å images taken between 18:14:54 and 23:37:26UT on June 09. Images were obtained at 30s cadence with an exposure time of 0.15s. The spatial sampling of these data is $0.109''$/pixels over a $111.6'' \times 111.6''$

FOV. To estimate the statistical noise in Ca II in §5.2 we use a very high cadence (8s) time-series of a plage region obtained on 2007, February 20, between 11:57 and 13:37UT. All the Ca II data were processed using FG_PREP.

TRACE also repeatedly observed AR 10960 during its passage across the disk, and movies of the region have been presented in Paper 1 and Paper 2. In §3 we use a 171 Å filter image obtained at 14:37:23UT on June 09 to identify the moss areas. The FOV was $512'' \times 512''$ and the exposure time was 32.8s. We also use a 1600 Å filter image obtained at 14:36:09UT to coalign with the SP data. The exposure time for this image was 0.86s. The data were processed and despiked using the *SolarSoft* routine TRACE_PREP. In addition, we use an XRT Open/Ti-Poly image taken at 14:34:46UT with a $512'' \times 512''$ FOV and 0.06s exposure time. This image was processed using XRT_PREP.

In section §6 we use EIS data to measure the moss filling factor. The EIS instrument is described in detail by Culhane et al. (2007) and Korendyke et al. (2006). It observes with high spectral and spatial resolution (22.3mÅ and $1''$ pixels, respectively) in short and long wavelength bands in the ranges 171–212 Å and 245-291 Å. Several slits from $1''$ to $266''$ wide are available for making observations. In this paper we use a raster scan obtained with the observing sequence AR_velocity_map at 10:58:10UT on June 09. The sequence runs for about 5 hr 15 mins and takes a context image by stepping the $40''$ slit across a large FOV followed by a $1''$ slit scan over $330'' \times 304''$. We only use the $1''$ slit scan data here, the exposure time for which was 40s at each position. Many lines are included in the study, though we only need one density diagnostic line pair for our analysis. The data were processed using the default options in the *SolarSoft* routine EIS_PREP. Each of the lines used were then fitted with Gaussian profiles to obtain the line intensity. Further details are given in §6.
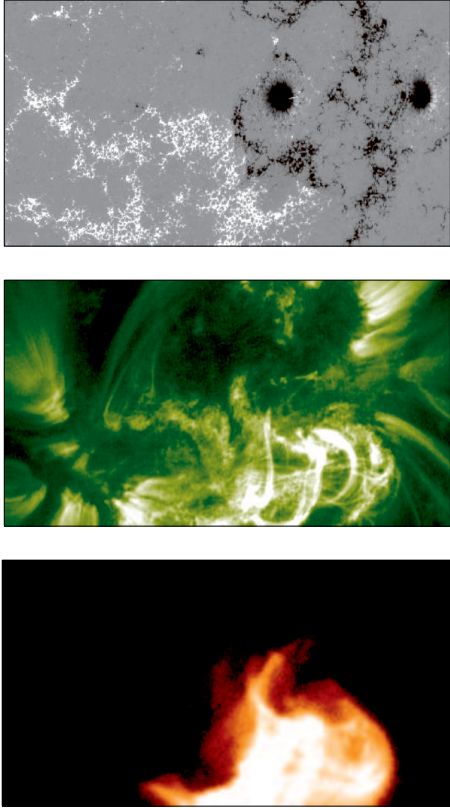
Fig. 2.— SP, *TRACE*, and XRT images of AR 10960. Top Panel: *Hinode* SOT/SP map corresponding to the FOV shown in Figure 1. The image shows the magnitude of Stokes V signal in the Fe I 6302 Å profile. Middle Panel: Coaligned *TRACE* 171 Å filter image taken at 14:37UT during the SP scan and showing the moss emission. Approximately coaligned XRT image taken at 14:35UT during the SP scan and showing the location of the high temperature core emission.
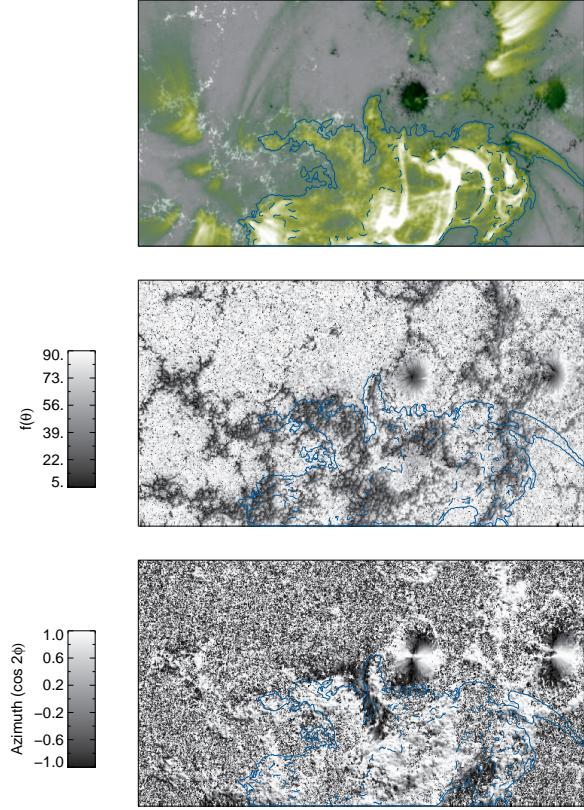
Fig. 3.— Coaligned SP and *TRACE* overlay, magnetic field inclination, and azimuth angle Top Panel: *TRACE* image overlaid in green on the SOT/SP map. The *TRACE* image has been scaled logarithmically. The solid blue line outlines the major moss region and the dashed blue line is intended to exclude obvious loop emission. Middle Panel: $f(\theta)$, where θ is the inclination angle. Lower Panel: $\cos 2\phi$, where ϕ is the azimuth angle. The same contours from the upper panel are overlaid in blue on the middle and lower panels.

3. Magnetic Characteristics of AR 10960

Here we describe the overall magnetic structure of AR 10960. To understand the relationship between the moss and the magnetic field we need to coalign the *TRACE* image to the SP large FOV map. To do this, we first cut out the common area from the *TRACE* 1600 Å image as determined from the FITS header coordinates. We then re-sampled the SP data to the lower *TRACE* resolution (note that all of the quantitative analysis is done on the original data), and then coaligned the 1600 Å image with the SP measured non-directional magnetic field strength. From this procedure we corrected the uncertainty in the common area of the 1600 Å image determined from the FITS header coordinates. We then extracted the correct area from the 1600 Å image.

This procedure worked well, but some stretching and rotation of the 1600 Å image compared to the SP map was evident as a result of the difference in plate scale magnification and satellite orbital attitude. These effects were corrected after visual inspection. The rotation correction is approximately 1° counterclockwise and the magnification correction is approximately 2% between the *TRACE* and SOT images. Furthermore, an E-W pixel shift of about 2 pixels was identified and removed.

Having established the alignment between the SOT and 1600 Å images, the coalignment with the 171 Å *TRACE* image was finally made by cross-correlating the two *TRACE* images after

the 171 Å image had been corrected for the inter-*TRACE* filter offsets reported by Handy et al. (1999).

Figure 1 shows full disk images taken on June 09 by the *SOHO* Extreme ultraviolet Imaging Telescope (EIT, Delaboudiniere et al. 1995) and Michelson Doppler Imager (MDI, Scherrer et al. 1995). The FOV of the *TRACE* data used to coalign with SOT is shown on the EIT image, and the FOV of the SP large FOV scan is shown on the MDI image. The extent of the active region and magnetic configuration are easily seen. Note the relative lack of complex emission or obscuration of the moss in the core of the region. This makes this particular region an ideal candidate for study.

Figure 2 shows the magnitude of Stokes V signal measured in the Fe I 6302 Å line, a coaligned 171 Å *TRACE* image, and an XRT Open/Ti-Poly image. The region is $\beta\gamma$ by June 09, with well separated positive and negative polarity flux. There is strong moss emission above both polarities in the core, separated by a dark channel above weak magnetic flux. As pointed out previously by others (Katsukawa & Tsuneta 2005; Tripathi et al. 2008; Brooks et al. 2008; Title 2009), the plage and moss areas are predominantly unipolar with unmixed flux, though the spatial correlation between the fine detail is not clear (Berger et al. 1999a; de Pontieu et al. 2003). There is bright loop emission to the south that obscures part of the moss. The XRT
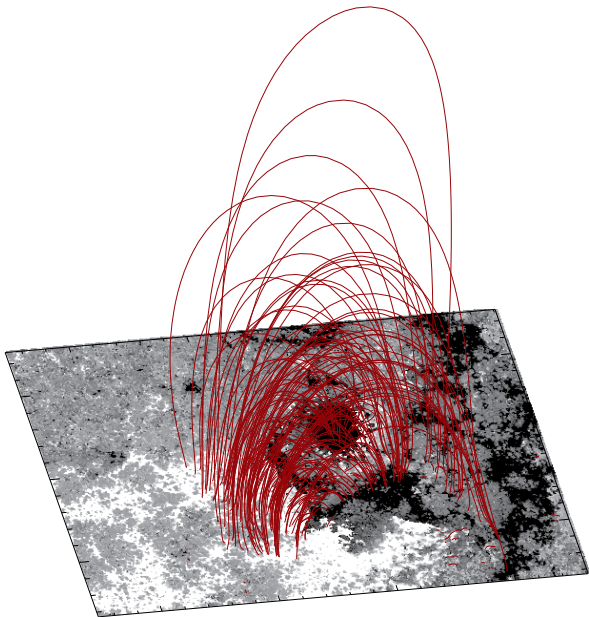
Fig. 4.— Potential field extrapolation from the moss region indicated in Figure 2. Only 218 field lines are shown for clarity.

image shows that hot loops surround this area with core emission around the sunspots and covering the moss. The detailed relationship between warm and hot emission in this region was investigated in Paper 2.

The results of the detailed coalignment between *TRACE* and the SOT/SP map are shown in Figure 3. An overlay of the 171 Å image on the SP data is shown in the top panel. We identified the major moss emission visually with a contour level ∼25% of the brightest loop emission in the 171 Å image. This is shown by the solid blue line. Within this region, there is clearly bright loop emission. To exclude these structures, we drew another contour at the 45% level (dashed blue line). The pixel coordinates of all points inside the moss contour but outside the dashed region were recorded for all the images. From here on when we refer to the moss region, this is the area we are referring to.

The magnetic field line inclination (θ) and azimuth angle (ϕ) in the region are shown in the middle and lower panels of Figure 3 with the same contours overlaid. In spherical coordinates, the field line inclination is along the line-of-sight so that an angle of 0° is directed towards the observer, and an angle of 180° is directed away from the observer. This will be relative to a radial field-line provided that the line-of-sight is normal to the surface, for example, when an active region is at disk center. For the data shown, the active region was at $\sim 30^o$ West of disk center.

The inclination angle in the figure is represented by the function

$$f(\theta) = \left\{ \begin{array}{ll} \theta & \text{if } \theta < \pi/2 \\ \pi - \theta & \text{if } \theta \geq \pi/2 \end{array} \right. \qquad (1)$$

This image shows large values of the inclination as white, and smaller values as black.

It has been pointed out previously that the magnetic field line orientation can be almost vertical to the solar surface (Katsukawa & Tsuneta 2005). The field rooted in the moss in this region appears to be only moderately inclined, with strongly in-

clined field mostly around the edges of the moss or in the inter-moss lane. It is also notable that the inclination is coherent, i.e., there is no obvious mixing of widely differing inclination angles.

The azimuth angle of the field is of course difficult to interpret because of the 180° ambiguity. For these data, the angle is measured from 0 to 180° from the Solar West position (RHS), but the value of the angle could be 180° in the opposite direction. Therefore, following Kubo et al. (2007), we show a $\cos 2\phi$ representation in Figure 3. This representation shows magnetic field oriented East-West as white, and field oriented North-South as black.

The strong moss emission is characterized by field oriented East-West in both polarities. The orientation again seems coherent, with the field mostly changing direction around the edges of the moss. The edges then, would be the places where most of the shear in the magnetic field is located. The strongest shearing is close to the inter-moss region where the field is predominantly oriented North-South.

4. MODELING

It has previously been noted that the large scale pattern of TRACE 171 Å brightness in the moss evolves slowly, with dynamics of motion and variability mostly on small-scales (Berger et al. 1999a,b). Brooks et al. (2008) noted that although there was fine scale variability in the magnetic flux below the moss in the region they studied, the general pattern also evolved slowly. In this paper, we assess the stability and evolution of the magnetic flux and vector field in AR 10960, but we also put our statements on a quantitative basis by comparing the observed time-scales to typical loop cooling time-scales computed from hydrodynamic simulations. Loop lengths vary throughout an active region, and since the radiative and conductive cooling times for a loop are dependent on the loop length, we first determined the distribution of lengths for loops relevant to the moss region using potential field extrapolations. The real magnetic field in the solar atmosphere is not likely to be current free (see e.g. De Rosa et al. 2009), however, the results from §3 show that the magnetic field is sheared mostly in the inter-moss region and that the field in the moss itself is unsheared with a small inclination angle. Since the moss is also unipolar, the field should escape almost vertically to the solar surface since it has nothing to connect to locally even if the field were non-potential. The potential field approximation, therefore, may be less problematic in the moss itself. In any case, the extrapolation is only used here to provide a realistic distribution of loop lengths.

A magnetogram for extrapolation was prepared by weighting the SP magnetic field strength by the magnitude of the Stokes V signal. The weighting determines the polarity of the flux. An area of $208'' \times 160''$ around the core of the active region was then extracted. Field lines were computed for every pixel in the magnetogram with a field strength between 5 and 5000G. Field lines rooted outside the moss region or that left the computational domain were then discarded. This resulted in a final dataset of 23917 field lines. A subset of 218 are shown in Figure 4 overlaid on the magnetogram.

An interesting result from this simulation is that the connectivity of the magnetic field in the moss is somewhat different than that of the quiet Sun. Close et al. (2003) showed that approximately 50% of the magnetic flux closes within 2.5Mm in the quiet Sun, with only 5–10% extending to heights greater
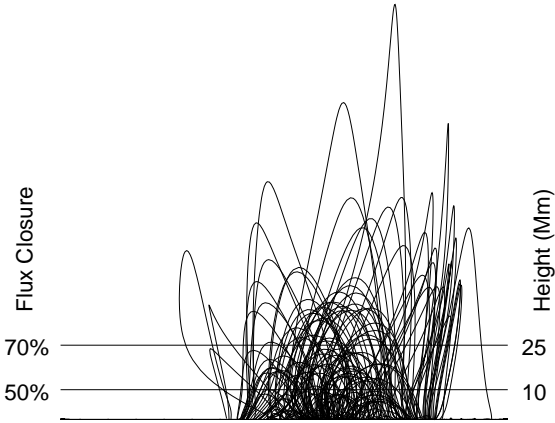
Fig. 5.— Rotated view of the potential field extrapolation of Figure 4 showing that, in contrast to the quiet Sun, most of the moss field connects to the corona.
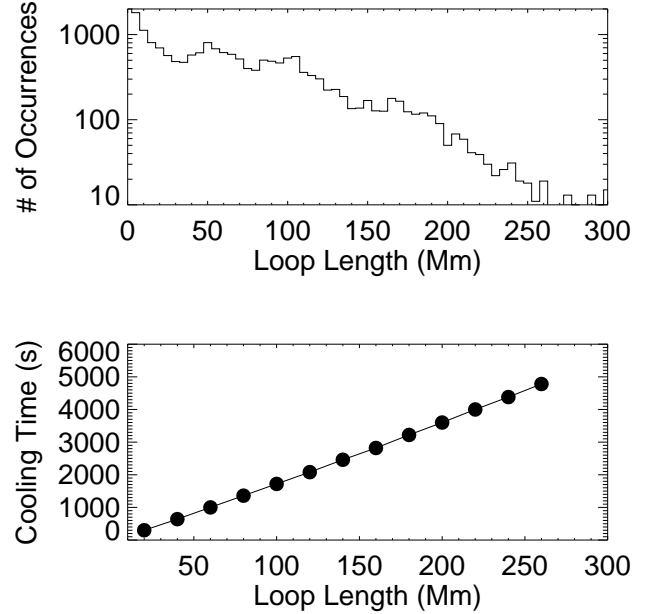

Fig. 6.— Top Panel: Distribution of loop lengths from the potential field extrapolation for all closed field lines in the moss regions. Bottom Panel: Loop cooling time versus length calculated by SOLFTM for the distribution of lengths in the top panel. Definitions are in the text.

than 25Mm. As mentioned, the magnetic field in the moss has nothing to connect to locally in the unipolar regions, so it can extend higher. Figure 5 shows a side-view representation of our simulation with the height extension and flux closure percentages indicated. Considering only the field lines rooted in > 20G field (approximately comparable to the simulations of Close et al. (2003)), we find that about half extend beyond 10Mm with a significant fraction (30%) extending to 25Mm and above. Many of the shortest field lines in our simulations are around the edges of the moss or crossing the inter-moss region. In these regions the potential field extrapolation is less likely to accurately represent the real sheared vector field, so the fraction of moss field lines that extend to significant heights is probably higher. This suggests that the moss is different than the quiet Sun in that most of the magnetized chromosphere is in fact connected to the corona. As we have shown (§3), this is also consistent with SP observations that the departure from the radial field line direction is only moderate.

The distribution of loop lengths for the full 23917 moss extrapolated field lines is shown in Figure 6 (upper panel). The distribution shows significant numbers of short (< 30Mm) field lines and populations in the range 30–80Mm and 80–120Mm. The maximum length is 337Mm. To compute cooling times for the moss loops we prepared a grid of lengths spanning a wide range up to 260Mm for input into the hydrodynamic code. For this simulation, we used the NRL Solar Flux Tube Model (SOLFTM) described in detail by Mariska (1987) and Mariska et al. (1989). Each loop on the grid was allowed to cool from a starting equilibrium temperature of ~ 4.8MK. The apex temperature at each computational time step is computed by averaging over the loop top. The loop is considered to have "cooled" when it reaches 1MK. This is close to the formation temperatures of Fe IX and Fe X, the spectral lines of which contribute significantly to the *TRACE* 171 Å pass-band. The result of the simulation is shown in the lower panel of Figure 6. The cooling times range from 300s for the shortest loops in the simulation, to 4800s for the longest loops. A linear fit to the results gives a relationship

$$t_c = -127.7 + 18.7L \qquad (2)$$

where L is the loop length, and t_c is the cooling time from 4.8 to 1MK.

5. VARIABILITY AND EVOLUTION OF MAGNETIC FIELD AND CHROMOSPHERIC EMISSION

5.1. Magnetic Flux

The time-series of FG magnetograms taken on June 09 was used to assess the variability of the magnetic flux in AR 10960. For this global look, we co-registered the time-series using cross-correlation on resampled (half dimension) data. We then calculated the average and standard deviation of the magnetic flux in each pixel over the whole time-series; $|\bar{B}|$ and $\bar{\sigma}$, respectively. We then calculated the quantity $\bar{\sigma}/|\bar{B}|$, that gives a measure of the variability in each pixel throughout the observations. This is over-plotted in red on $\bar{B}$ in Figure 7 so that the locations of high and low variability in the region can easily be distinguished. Note that since B is averaged over the whole time-series, $\bar{B}$ highlights the areas where the magnetic flux persists. Only the points were $\bar{B}$ is above the estimated statistical noise (see below) are plotted.

As one would expect, the magnetic flux is persistent in and around the strongest field. It can also be seen that the variability is highest away from these regions. In particular, the variability is low in the moss and high around the edges. It is also high around the neutral line that passes through the inter-moss lane. In previous studies it has been shown that most transient brightening activity in the EUV occurs around the neutral line of an active region, and that the magnetic flux pattern is persistent around the bases of high temperature loops (Brooks et al. 2008). This plot is consistent with that picture.

The movie (movie1.mpg) associated with Figure 7 shows the spatial distribution of the magnetic flux evolving slowly. To quantitatively asses this evolution we computed the linear Pearson cross-correlation coefficients, r, between magnetograms separated by varying time-intervals. The Pearson coefficient is calcu-
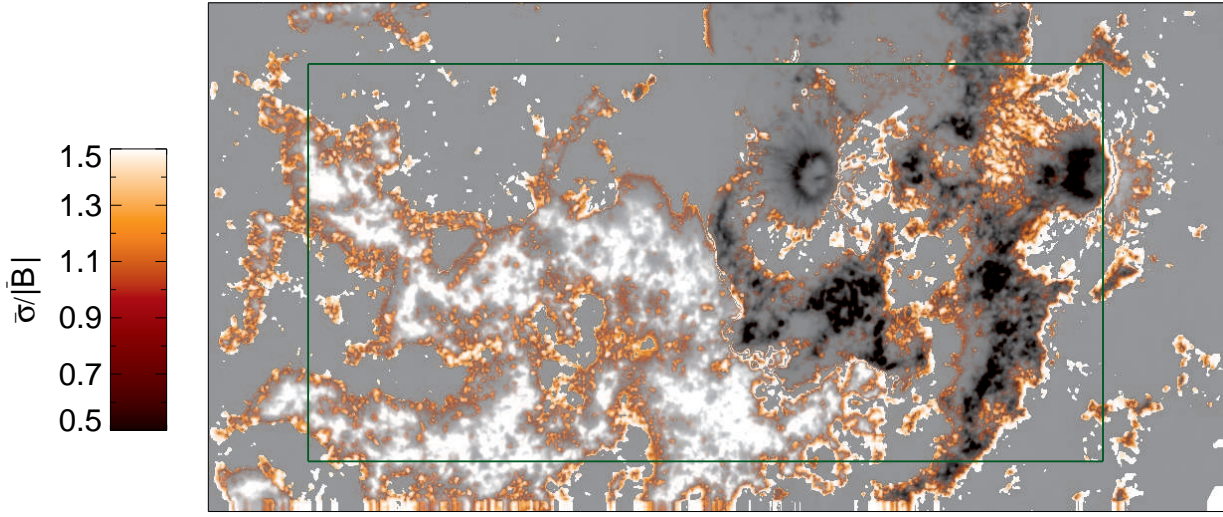
Fig. 7.— Plot of $\bar{\sigma}/|\bar{B}|$ overlaid in red on $\bar{B}$ for each pixel in the complete time-series of SOT/FG data. The solid green line shows the area used for the cross-correlation results of Figure 8. Only the points where the magnetic flux is above the estimated statistical noise (16.6G) are shown. A movie of the complete series of magnetograms is available in the electronic edition of the manuscript as movie1.mpg.

lated by dividing the covariance of two images by the product of their standard deviations, and was computed here for the boxed green area indicated in Figure 7 using the IDL routine CORRE-LATE. Since each magnetogram is separated by only 30s, r will be very high if the time-interval between them is small. As the separation is increased, the correlation will begin to break down because of the evolution of the spatial distribution of the flux. The data are interrupted by *Hinode* night time every orbit, so the cross-correlation is made only between magnetograms taken in the same orbit.

Figure 8 shows the results. For magnetograms taken at 30s frequency r is close to 1.00 for the duration of the time-sequence, indicating a strong correlation between successive magnetograms as expected. As the separation between magnetograms is increased to 120s r falls, but is still maintained close to 0.98. With a separation of 960s r is close to 0.94, and with a separation of 1920s r is maintained close to 0.90. 1920s is equivalent to the cooling time for a loop of length 110Mm in our hydrodynamic simulations. Since 85% of the loops in our field extrapolation are shorter than this they cool from ~ 5 to 1 MK on shorter time-scales. This indicates that the spatial distribution of the magnetic flux maintains a strong correlation for time-scales longer than the cooling times for *at least* 85% of the loops extrapolated from the moss regions. With the data at hand, it is not possible to assess the pattern of magnetic flux over longer time-scales.

The variation of the magnetic flux in small areas as a function of time was then investigated. The analysis is not sophisticated. We used the full resolution data and extracted a 1000 pixel^2 area from each magnetogram. This time-series was then co-registered via cross-correlation of successive magnetograms. Figure 9 shows one of the FG magnetograms in the time-series. Eleven small boxes are overplotted scattered throughout the positive and negative polarity moss regions. One in the inter-moss

region is also included. The boxes are $2''\times2''$. This size was chosen because it is comparable to the spatial resolution of EIS, which was measured to be close to $2''$ in the laboratory pre-launch (Korendyke et al. 2006). It is about the same size as a low resolution MDI pixel.

In order to understand whether the variations in small areas are significant or not, we need to estimate the statistical uncertainty. Since the FG does not do a full magnetic vector inversion we cannot quantify the various sources of noise. Therefore, we adopted the following approximate method. We selected a relatively quiet region, shown by the large box in Fig 9, and formed histograms of the difference in magnetic flux per unit area between successive magnetograms in the time-series. These histograms were then fitted with Gaussian functions and the standard deviation (σ) measured. The standard deviations are plotted as a function of time in the upper left panel of Fig 10. The average value is 16.6G with $\sim 15\%$ variation in the standard deviations as a function of time. We adopt this average value as our estimate of the statistical noise. There may be signals below this value, but they would be difficult to reliably distinguish from noise, with the caveat that the quiet region selected is in an active region so is only 'relatively' quiet. It is likely that the true statistical noise level is lower. This estimate should be taken into account when considering the results for the moss and inter-moss regions below.

Figure 10 shows the results of this analysis. The interpretation is complicated because it is difficult to distinguish changes in the magnetic flux due to features evolving, or moving in or out of the field of view. As noted by Brooks et al. (2008), the constancy of the spatial distribution of magnetic flux in an active region can be preserved by magnetic features moving along similar paths, i.e., the field is dynamic, but the pattern is maintained. We are interested, of course, in the evolution of features,
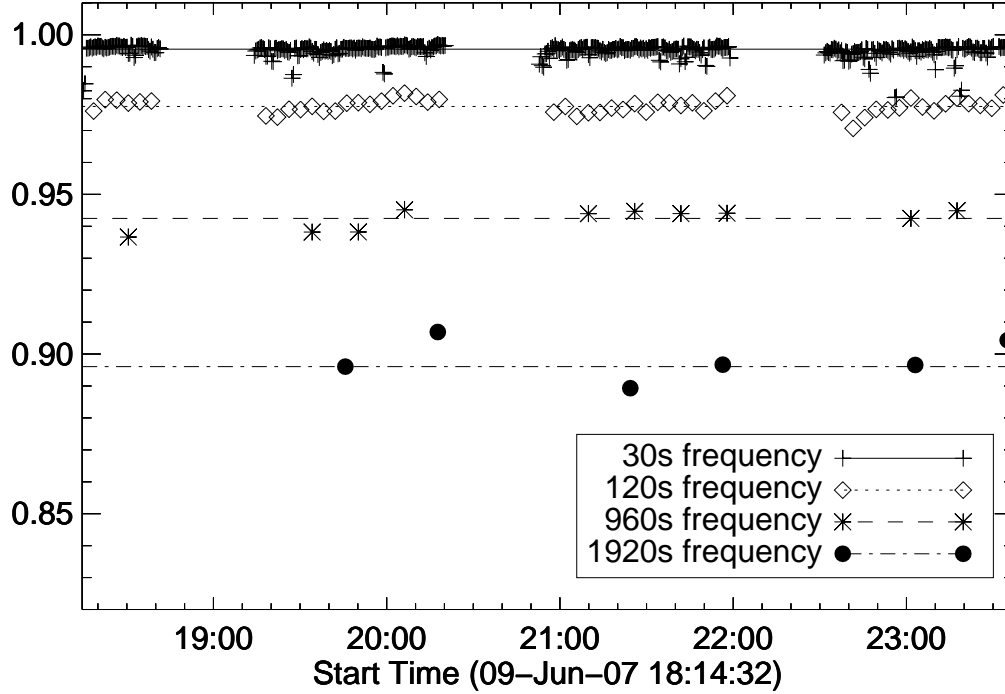
Fig. 8.— Variation of the linear Pearson correlation coefficient between magnetograms separated by varying time-intervals as a function of time. The correlation is made between time-series with magnetograms taken at frequencies of 30s, 120s, 960s, and 1920s. The last value is equivalent to the cooling time for a loop of length 110Mm.

but also want to eliminate cases where we end up tracking something else. We have therefore made an effort to select regions where obvious motions in or out of the box are reduced. The movie (movie2.mpg) associated with Figure 9 allows the reader to independently judge this analysis.

The positive polarity moss box in the top row of Figure 10 shows an average magnetic field of 510G and around 22% variation over the duration of the observations ($>$ 5 hr). This is clearly much longer than the theoretical cooling times. The negative polarity moss box in the top row shows a comparable average magnetic field of -490G and $\sim$ 27% variation during the observations. The majority of the boxes in Figure 10 show fluctuations around this level of 15–30%. These values for the moss are a little higher than the results found for coronal intensities and velocities in papers 1 and 2. A few cases show larger variations at the 40–50% level, but it is clear that this also reflects the fact that the magnetic flux is evolving slowly. Note, for example, the box in the lower right panel of Figure 10. This box shows a variation of $\sim$45% during the observing period. This is a result, however, of a slow evolution from around -550G at 18:30UT to around -200G at 23UT rather than a sudden change. In fact, even in this box, a less than 30% variability is maintained if we consider just the first, or last, 3 hours of observations. If we consider only the first hour of the observations the magnetic flux in all of the boxes varies by less than 10%. This is still considerably longer than most of the simulated loop cooling times: only loops longer than $\sim$200Mm persist for an hour, and only about 2% of the loops in our simulation are this long.

The inter-moss region shows an average magnetic field of 15G and the highest variation of all the boxes ($\sim$ 60%) This is con-

sistent with our expectations since the inter-moss region was already identified as being more variable in Figure 7. As pointed out earlier, transient EUV brightenings have been found to be preferentially located around the neutral lines in other active regions. The inter-moss region also seems to be where the majority of the flares and transients occur in this region (see, e.g., the *TRACE* movies in papers 1 and 2).

Some areas of the moss do show evidence of dynamic changes in magnetic flux similar to that in the inter-moss box. Also, it is unclear how significant 15–30% variations in moss magnetic flux are over time-scales of several hours. Variations comparable in magnitude do occur on shorter time-scales (tens of mins). These changes are on the order of 100–200G and are statistically significant. Therefore, they could be taken as evidence for low-frequency impulsive heating. Note that changes on 20–30 mins time-scales correspond to the cooling times for loops in the 70–100Mm range. We find, however, that only a small fraction ($\sim$10%) of our simulated moss loops would be expected to cool on these time-scales. This suggests that such heating is not significant here, and may also be consistent with the lack of "warm" EUV loops cooling in the core of this region.

The 100-200G magnetic flux changes correspond to $\sim 10^{18}$Mx in the boxed regions, and would be equivalent to smaller than micro-flare size energy releases in the corona. Further work is needed to see if these could be related to, or signatures of, the flare-like intensity variations intermittently seen in hot X-ray core loops (Warren et al. 2007) or hot transient events (Shimizu 1995). Here we focus on determining whether such variations show evidence of propogating energy into the chromosphere.
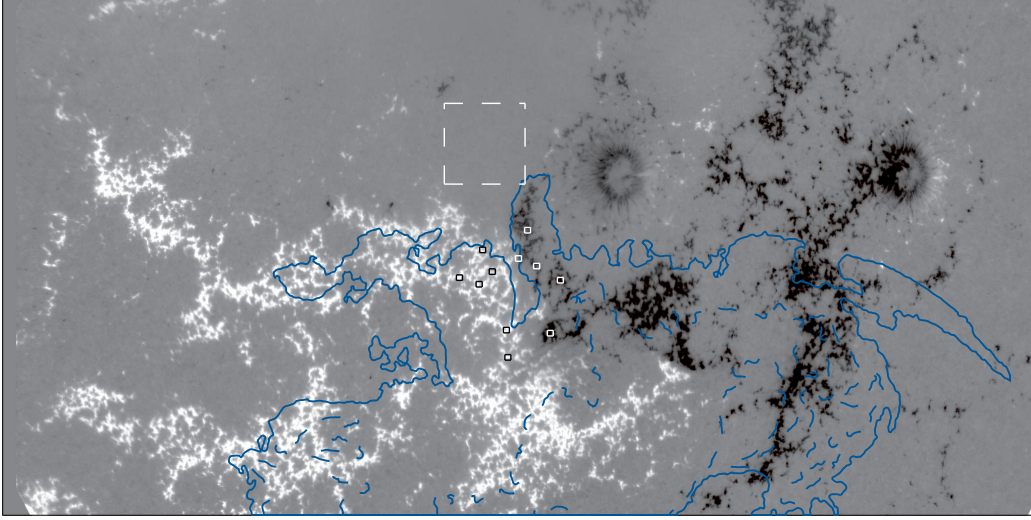
Fig. 9.— FG Na I 5896 Å magnetogram taken at 18:14:32UT on 2007, June 09. The large dashed box is the control region used for estimating the statistical noise (see text). Eleven small boxes are also overlaid and the variability of the magnetic flux in these regions as a function of time is plotted in Figure 10.

5.2. *Ca II H Intensity*

The variation of chromospheric emission in the Ca II 3896 Å line as a function of time was investigated using the time-series of images taken on June 09. The time-series was co-registered to the first image by cross-correlating successive images. Figure 11 shows an example image taken at 18:14:55UT with the same eleven small boxes and large control box as in Figure 9 overlaid. The placement of these boxes was made by determining the inter-FG offsets and scalings by co-registering this Ca II image with a near-simultaneous Na I D magnetogram. This was achieved by cross-correlating a common area from the two images and re-sampling the magnetogram to the higher resolution of the Ca II image.

As with the magnetic flux analysis, we need to estimate the statistical uncertainty in order to gauge whether variations in the Ca II emission are significant. For this purpose we analysed a time-series of very high cadence (8s) Ca II images of a plage region obtained between 11:57 and 13:37UT on 2007, February 20, with an exposure time of 0.41s. The data were co-registered by cross-correlating successive images and intensity difference images for the entire time-series were prepared. Histograms of the intensity differences over the full FOV ($56'' \times 28''$) were then formed for each image in the time-series and fit with Gaussian functions to determine the standard deviation (σ). The standard deviations are plotted as a function of time in the upper left panel of Fig 12. The average value is 9DN/s with only 4% variation in the standard deviations as a function of time. We adopt this average value as our estimate of the statistical noise.

Figure 12 also shows the variation of intensity in the moss and inter-moss boxes. An animation (movie3.mpg) shows the locations of the boxes, and their stability, during the time-series. Remarkably, the average intensities in all the boxes (including the inter-moss box) are within 10% of each other. Furthermore, the intensity variation is less than 10% in all the boxes for the duration of the observations (> 5 hours). The largest variation can be seen in the lower left hand box. As with the magnetic flux, this is again clearly a slow evolution from ~ 1200DN/s at

the start of the sequence to ~ 900DN/s at the end. Comparable magnitude variations of 100–200DN/s are again seen on time-scales of tens of minutes, and these are significantly above the noise estimate.

We computed the correlation coefficients between the Ca II intensities and magnetic fluxes for each of the boxes. Intriguingly, about half show a correlation coefficient > 0.5, indicating a weak positive correlation and suggestive that the 100–200G changes in the magnetic flux do propogate energy and heating that leads to emission that is detectable above the noise level in the chromosphere, though it is not universally seen. Sakamoto et al. (2008) have recently also reported the detection of fluctuations in *TRACE* 171 Å observations above the photon noise level that have durations that agree well with their estimated loop cooling times, albeit for a different active region. Our analysis of EIS 195.119 Å observations of this region (paper 1) showed only $\sim 15\%$ variations in intensity over many hours, but a detailed comparison with the noise was not made. The lack of a consistent detectable signature in the chromosphere and a possible signature in the *TRACE* data could indicate that the energy propogation is amplified in the corona, or is in fact released there. Further work on this issue is warranted, including comparisons of intensity variations with numerical models (Antolin et al. 2008).

5.3. *Magnetic Field Vector*

Figure 13 shows the same magnetic field inclination map represented by $f(\theta)$ as in Figure 3 and defined in Equation 1. The FOV of the narrow ($7'' \times 512''$) SP slit scan from June 08 is overlaid. The FOV has been rotated to the time of the large FOV scan (14:20 on June 09). The same 171 Å contours as before are shown. It can be seen that the narrow scan crosses the inter-moss region South-North and reaches both positive and negative polarity moss regions. Both regions also appear to be moderately inclined to the line-of-sight (black) whereas inter-moss region shows strong inclination (white). Two regions are selected in the moss (the small boxes within the FOV in Figure 13) to study the variation of the field line inclination and azimuth angle. The
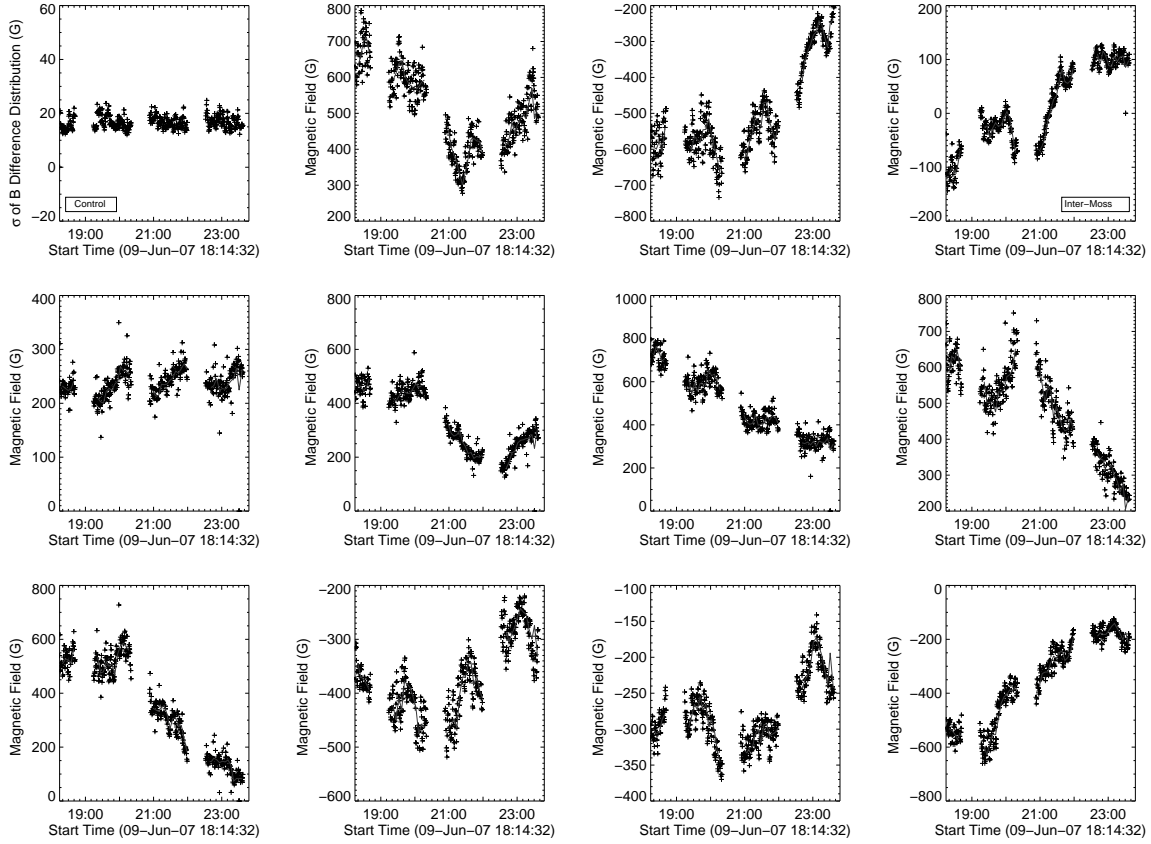
Fig. 10.— Variation of moss magnetic field - flux per unit area - in Gauss (G) as a function of time. Top left: standard deviation of histograms of the pixel-to-pixel difference between successive magnetograms in the control box shown in Figure 9. Other panels: evolution of the magnetic field averaged over the small boxes in Figure 9. The crosses show the individual points, and the thick solid lines show detrended 5 mins averaged curves to de-emphasize the scatter.
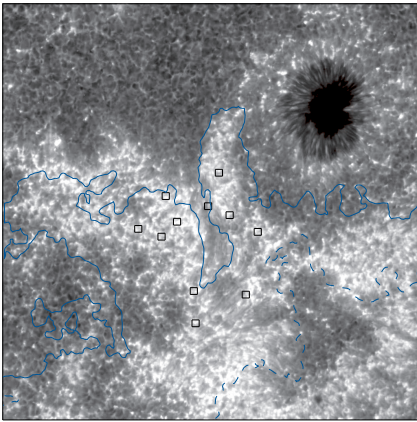
areas of the boxes are again $2'' \times 2''$.

Fig. 11.— FG Ca II 3896 Å magnetogram taken at 18:14:54UT on 2007, June 09. Eleven small boxes are overlaid and the variability of the Ca II intensity in these regions as a function of time is plotted in Figure 12. The moss contours from Figure 3 are overplotted in blue.

Figure 14 shows the results. Consistent with the measurements in §3 both moss regions show moderate inclination from the line of sight with an average value of 27°. The variation is less than 15% over the time-series (21:56:03–22:59:31UT). The azimuth

angle changes from $\sim 120^o$ at the start of the time-series to $\sim 90^o$ by the end, but as with other quantities, this is a slow evolution, and the variation from the average ($\sim 109^o$) is less than 15% over the whole period. Note that this time-series lasts for 3808s, which is again much longer than the theoretical cooling times for loops extrapolated from the moss regions calculated in §4.

One criticism of such simple analyses is that variability on small scales is smoothed out by the averaging over large areas. It is possible that coronal emission is quasi-steady over many hours on size scales at the limit of current EUV/X-ray instrumentation, but that future instrumentation will find higher variability on smaller spatial scales. What tends to happen is that quantities appear relatively steady for many hours, within some threshold, when averaged over large areas. These quantities also appear steady when averaged over smaller areas, but for shorter periods of time, though the duration can be extended if the threshold is relaxed. For example, the most variable quantity in Figure 14 is the inclination angle in the positive polarity box. It varies by less than 15% over the observations period. Individual pixels in this box, however, have larger variabilities: $\sim 34\%$ on average. Relaxing our definitions slightly, however, we are still able to say that $> 80\%$ of the individual pixels vary by less than 30% over time-scales comparable to the cooling times for 85% of the loops in our simulations (1920s).

The key question of course is how these time-scales, spatial scales, and thresholds, compare to the critical values for coronal
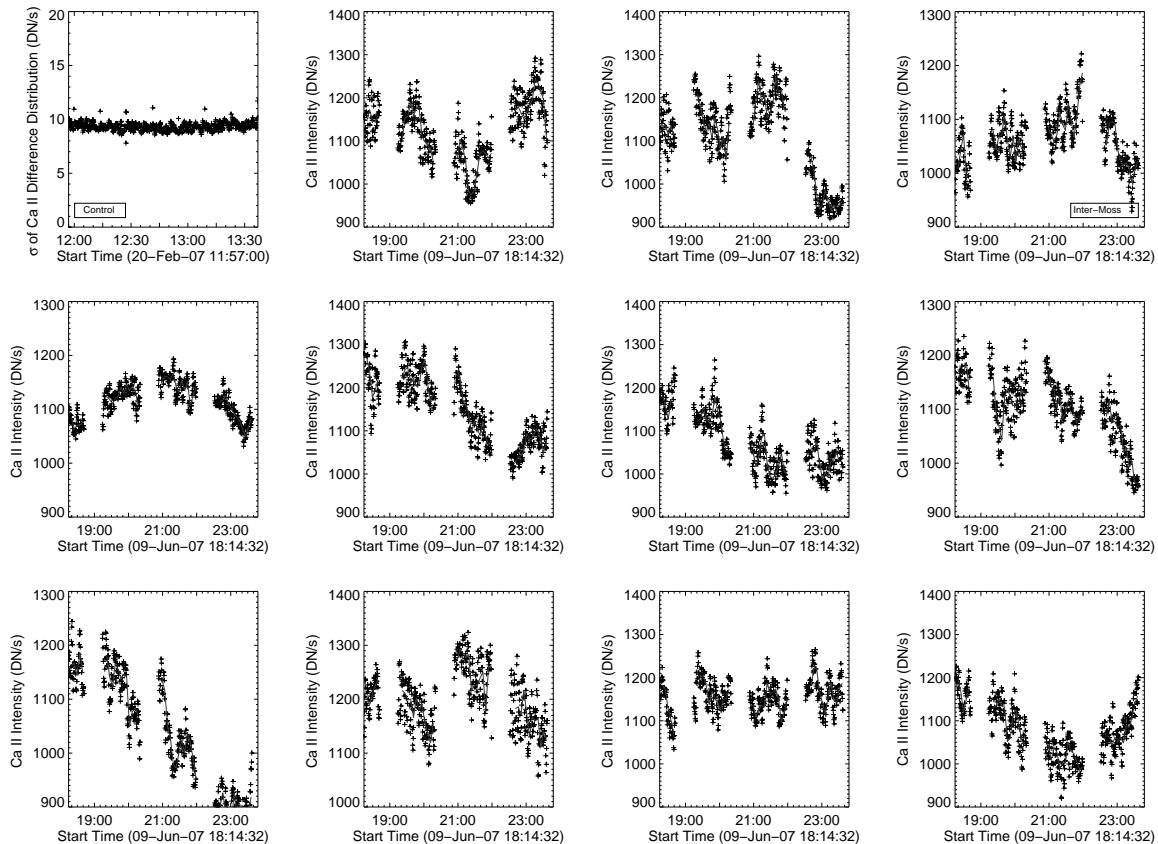
Fig. 12.— Variation of moss Ca II intensity (DN/s) as a function of time. Top left: standard deviation of histograms of the pixel-to-pixel difference between successive images in the control box shown in Figure 11. Other panels: evolution of the Ca II inensity averaged over the small boxes in Figure 11. The crosses show the individual points, and the thick solid lines show detrended 5 mins averaged curves to de-emphasize the scatter.

heating. We have shown that the chromospheric Ca II emission and all the magnetic activity in AR 10960 evolves slowly, and our quantitative analysis also indicates that the variability in magnitude is only at a low level on time-scales longer than theoretical loop cooling times in small $2'' \times 2''$ boxes. The movies presented in this paper clearly suggest, however, that there is a lot of small-scale dynamic activity. The time-scale for loop cooling is clearly resolved in these observations, but the important spatial scales may not be. Next we investigate the moss filling factor in this region using EIS observations in order to at least indirectly infer the size scale of a fundamental loop envelope.

6. EIS FILLING FACTOR MEASUREMENTS

Previous studies have shown that intensities in the moss scale linearly with the loop base pressure and independently of the loop length (Martens et al. 2000; Vourlidas et al. 2001). As pointed out by Warren et al. (2008b), this means that any physical model that yields the same base loop pressure will predict the same moss intensity regardless of the loop length. Warren et al. (2008b) calculated full solutions to the hydrodynamic equations, assuming steady heating, for a grid of loop lengths from 10–100Mm. This grid sufficiently covers most of the distribution of loop lengths we computed for the moss in §4. For each loop solution, the density and temperature around the loop is known and the intensity at each position for any EIS line can be calculated. By integrating the intensity over the lower 5Mm of the loop the footpoint intensity can be computed. The intensities for

the grid of loops scale linearly with pressure and can be fitted with a function of the form $I_\lambda = aP_0^b$, where I is the intensity and P_0 is the base pressure. Warren et al. (2008b) state that the linear relationship between intensity and pressure breaks down at low pressures, so their fits are restricted to values above log $P_e = 16$ cm^{-3} K.

The intensity ratios of selected lines can also be directly related to the simulated base pressure. By determining the moss pressure from observed intensity ratios, a simulated intensity for an individual line can be calculated from the fit and compared to the observed intensity for that line. The filling factor is then introduced (if needed) to bring the simulated and observed intensities into agreement. We followed this procedure here for AR 10960.

Following the analysis in paper 2 we use a density threshold to identify the moss pixels. Several density diagnostics are available in the EIS wavelength bands and a detailed discussion of comparisons between them has been presented in Young et al. (2009). In paper 2 we discussed these comparisons and decided to use the Fe XIII 202.044/203.826 Å ratio because of the consistency between densities derived from this ratio and densities derived from Si X ratios in small active regions, bright points, and the quiet Sun i.e. regions where the density is lower than in the moss and the Si X lines are sensitive. For comparison with that work, we use this ratio again here. The analysis is applied to the EIS slit raster scan taken at 10:58:10UT on June 09, and discussed in §2. The Fe XIII 202.044 Å line was fitted at every
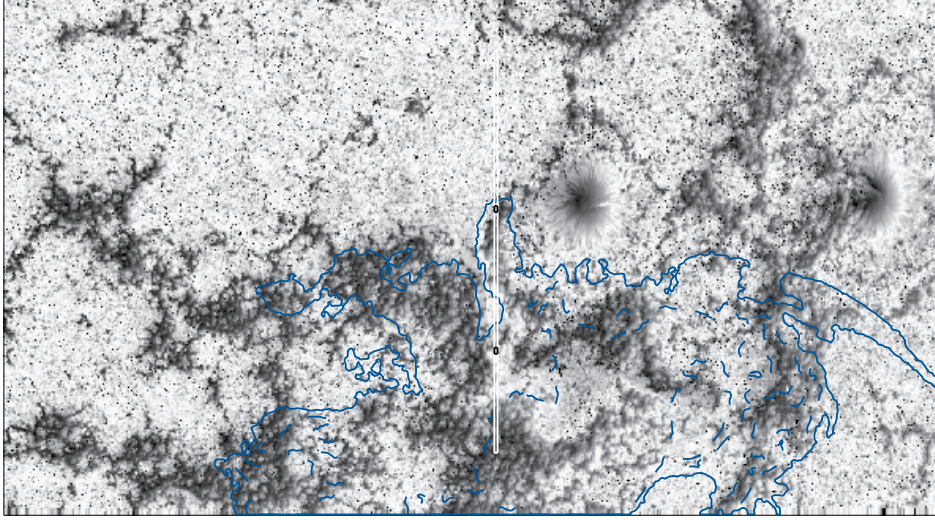
Fig. 13.— Magnetic field line inclination at 14:20:05UT on June 09 with the FOV of the narrow SP scan overlaid in white. The small black boxes within the FOV show the areas chosen for analysis in Figure 14. The contours are the same as in Figure 2.

pixel with a single Gaussian. The Fe XIII 203.826 Å line is a self-
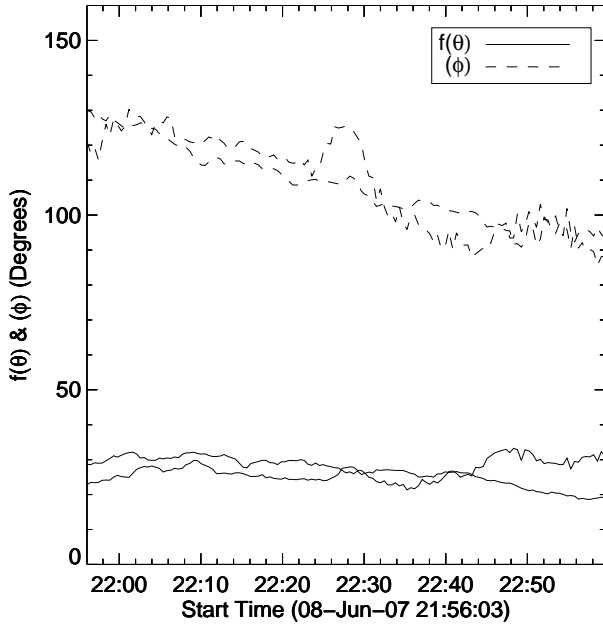

Fig. 14.— Variation of magnetic field inclination and azimuth angle as a function of time for the positive and negative polarity moss regions shown as boxes in Figure 13. The inclination is represented by $f(\theta)$ (see text). Less than 15% variation is seen in all quantities over a period of about 1 hr.

blend of two lines and is further blended at 203.734 Å with an Fe XII line (Brown et al. 2008). We performed a double Gaussian fit to this feature at every pixel to remove the Fe XII blend. To do this, we fixed the separation of the two components at 0.1 Å and forced them to have the same width.

Images of the active region core formed from the line fits are shown in Figure 15. The full raster spanned several passes through *Hinode* night, so the images only show a central area

of 80″×140″. Electron densities were calculated for these regions using the measured line ratios and the CHIANTI database version 6.0 (Dere et al. 1997, 2009). A contour set at 40% of the maximum intensity is drawn on the Fe XIII 203.826 Å image of Figure 15 to highlight the moss regions. Pixels within these contours were selected and identified as moss if the calculated electron density exceeded log N_e = 9.6 cm^{-3}. These are shown as crosses on the Fe XIII 203.826 Å image. For each of the identified pixels, the observed intensity ratio was computed after subtracting contaminant background emission. This background intensity was measured in the small box in the inter-moss region on the Fe XIII 203.826 Å image. The new ratios were then used to derive the base pressure by interpolation from the simulated grid of solutions. Figure 16 shows the values for the moss pixels overplotted on the theoretical line ratio vs base pressure curve. Although several moss pixels approach the high pressure limit of the ratio, it can be seen that the vast majority of them fall in the sensitive range of the curve. The minimum base pressure in the moss is log P_e = 16.3 cm^{-3} K, which is higher than the lower limit of the power law fits of Warren et al. (2008b). With the base pressure established, the Fe XIII 203.826 Å intensity was simulated using the fit for Fe XIII 203.826 Å. The coefficients of the fit in this case are a = -11.94 and b = 0.99.

As expected, the intensities thus simulated are much higher than observed, so a filling factor needs to be introduced to bring them into agreement. The distribution of filling factors for the moss pixels is shown in Figure 17. The majority of values fall in the 10–20% range with the median value being ∼16%. This is in agreement with previous measurements of moss filling factors (Fletcher & de Pontieu 1999; Warren et al. 2008b).

These results suggest that the fundamental size scale of structures in the moss are about 10–20% of the EIS spatial resolution. This is consistent with similar measurements of coronal loops with EIS based purely on observational factors (Warren et al. 2008a), and also sets an upper limit on the cross-field scale of coronal heating, which will be much smaller if loops are composed of multiple threads. Note that the filling factor is an area
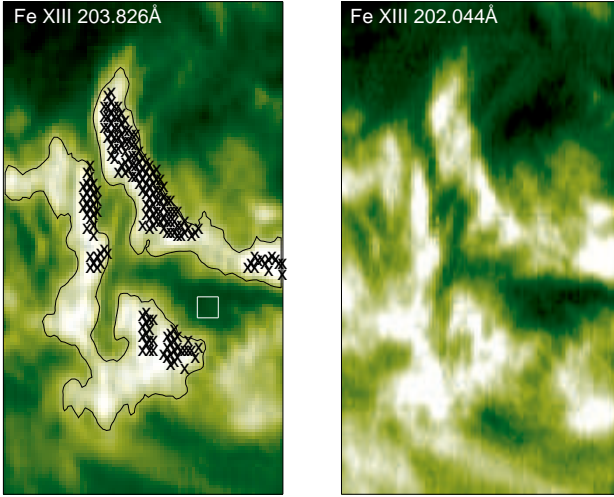
Fig. 15.— EIS images of the core of AR 10960 formed from fits to the density sensitive Fe XIII lines. The moss regions are highlighted by a contour at 40% maximum intensity. The small white box shows the inter-moss region used for background subtraction, and the crosses show the moss pixels with log $N_e > 9.6$ cm^{-3} used for determining the filling factor.
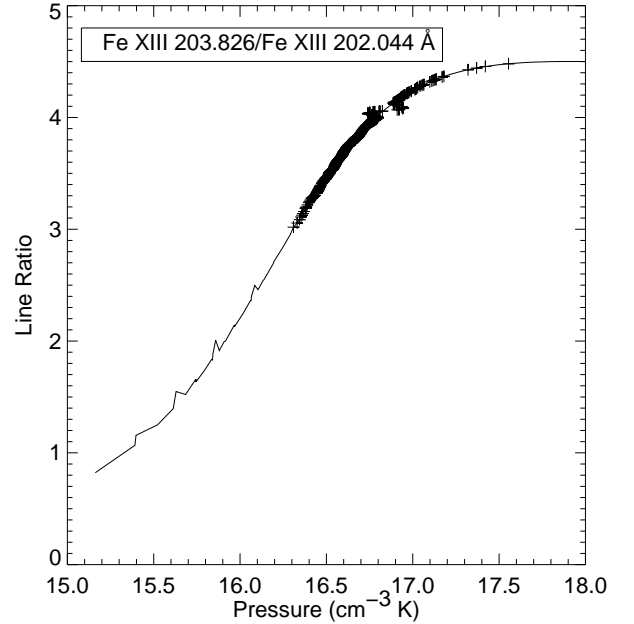

Fig. 16.— Theoretical line ratio versus base pressure curve for the grid of loop models discussed in the text. The values for the moss pixels highlighted in Figure 15 are overplotted as crosses.

filling factor. EIS has $1''$ spatial pixels, so taken at face value a next generation instrument needs 0.3–$0.4''$ spatial pixels to resolve the median moss filling factor. Interestingly, this is larger than the size of the SOT FG and SP pixel scales. Although EIS (and XRT) cannot directly resolve these scales, SOT can resolve these scales below the moss.

7. Magnetic flux evolution and chromospheric emission in individual pixels

Having inferred the apparent cross-field size scale of fundamental structures in the moss and established that the FG can resolve this scale in individual pixels, we revisit our analysis of the variability in magnetic flux and chromospheric emission in the moss region (§5). Previously we showed that the average magnetic field in most of the boxes varied by ~ 15–30% while the chromospheric Ca II 3896 Å intensity varied by $\sim$10%. Note that these changes include changes due to motions in and out of the field of view as well as variations in magnitude. These motions may have a more pronounced effect on the results for individual pixels because the features can traverse the pixel size scale faster. It is worth pointing out that features moving in and out of a pixel can have the effect of canceling each other to some degree so that variability may be reduced. This would also be true if the fundamental structures are composed of multiple threads.

Figure 18 shows the distribution of percentage variabilities (ratio of standard deviation σ to average magnetic field $\bar{B}$) for all the pixels in two of the boxed regions. Each box contains 156 pixels. The values are calculated for a time-period of 1920s. Recall that 85% of the loops in our simulation cool on shorter time-scales than this. In both cases $> 75\%$ of the pixels show variabilities less than 20% and the median values for both distributions are $\sim 13\%$. The variability is clearly greater in individual pixels over the full observations period, but this is also partly attributable to the lifetime of individual features. For the record, more than 2/3 of the pixels in the boxes show less than

45% variability for the whole > 5 hr period.

Figure 19 shows the distribution of percentage variabilities of the Ca II 3896 Å intensities for all the pixels in the same two boxed regions, computed for the same time-period. In this case, each box contains 306 pixels. In both cases $\sim 85\%$ of the pixels show variabilities of less than 10% and the median values for both distributions are $\sim 6\%$. Again, the variability is larger over the full observations period but, at least for the selected boxes, all the pixels show less than 15% variability for the whole > 5 hr period.

To check whether the two examples are representative, we show in Figure 20 the distribution of percentage variabilities of the Ca II 3896 Å intensities and unsigned magnetic flux for all individual pixels within all the moss boxes. The Ca II distribution has a median around 6% with 99% of the pixels showing variabilities of less than 15%. The median of the magnetic flux distribution is around 15% with more than 2/3 of the pixels showing variabilities of less than 20%. These values were again computed for a time-period of 1920s. As discussed in §5, the magnetic flux in the moss shows greater variation, but this does not seem to register strongly in the chromosphere.

8. Discussion

We have described the characteristics and evolution of the longitudinal and vector magnetic field and chromospheric Ca II emission in the core of an active region observed by *Hinode* and *TRACE*. Consistent with previous studies, we found that the moss in this region is unipolar, the field lines are only moderately inclined, and the spatial distribution of magnetic flux in the core evolves slowly. We put the last statement on a quantitative basis by comparing the evolution time-scales with the theoretical cooling times computed from hydrodynamic simulations of coronal loops extrapolated from SP magnetograms of the moss regions.
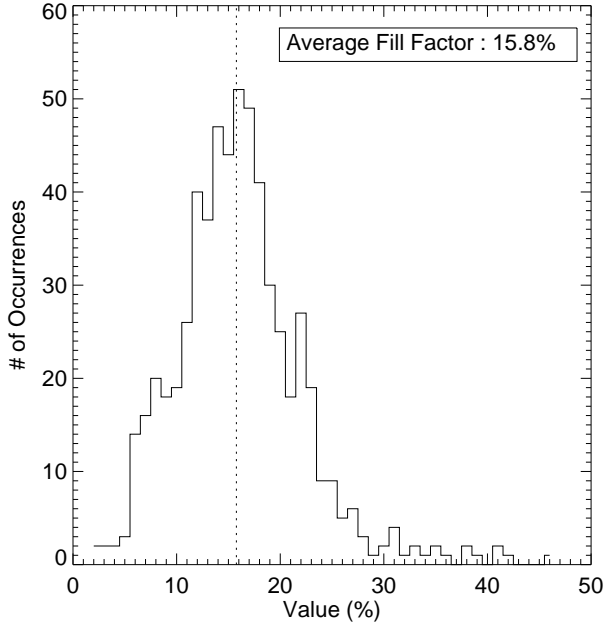
Fig. 17.— Distribution of filling factors computed for the moss pixels.

Fig. 18.— Distributions of magnetic field variability ($\sigma/\bar{B}$) expressed as percentages for the individual pixels within a positive and negative polarity moss box from Figure 9.

These extrapolations also showed that the magnetic connectivity in the moss is different than in the quiet Sun because most of the magnetic field extends to significant coronal heights (there is nothing to connect to locally in the unipolar regions). We also showed that the field line inclination and horizontal component are coherent in the moss, and most of the shearing of the field occurs in the inter-moss region, or at the edges of the moss, where the magnetic flux variability was shown to be greatest. The magnetic vector, flux, and Ca II intensity in $2'' \times 2''$ boxes in the moss also do not show significant variability on time-scales longer than loop cooling time-scales when averaged over these areas. Though flux changes on the order of 100-200G and Ca II intensity changes on the order of 100-200DN/s are observed on 20–30 mins time-scales, we find only weak evidence that these flux changes consistently register in the chromosphere. We also determined the filling factor in the moss from EIS observations: ~16%. This is consistent with previous studies, and suggestive that the cross-field scale of the fundamental structures in the moss are larger than the size of an individual SOT FG pixel ($0.16''$). The mean variabilities of the magnetic flux and chromospheric emission in individual FG pixels was also found to be ~15% and ~6%, respectively, on time-scales longer than the computed loop cooling times.

EUV and X-ray observations of the moss in the core of this region have already suggested that the heating is steady or effectively steady i.e. heating events occur with a rapid repetition rate. The results presented here show that the magnetic field and chromospheric emission also evolve slowly, and remain relatively steady even at the highest spatial resolution we have ever observed. They could therefore be interpreted as further evidence supporting the quasi-steady picture. The short time-scale 100-200G variations we see could be interpreted as evidence of low frequency impulsive heating. We find, however, that only a small fraction of our simulated loops (10%) would be expected to cool on these time-scales.
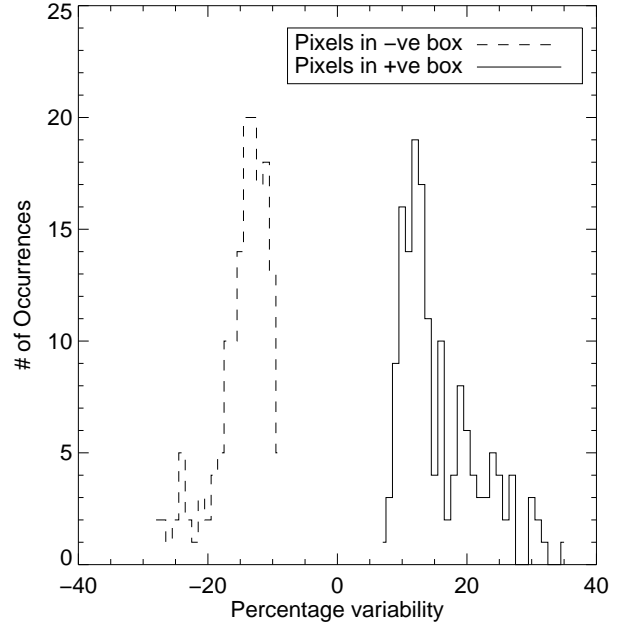
If the heating events do occur frequently and are reconnection related, one would also expect to see changes in the magnetic field on a comparable time scale. Further studies of the relationship between the detailed small scale changes in the magnetic flux that we see and variations in the EUV/X-ray intensities are needed to address this issue. At present it is unclear theoretically how important changes of 10–20% are in terms of energy input. The magnetic field inclination, for example, is indicative of the horizontal stress component of the field and could be directly realted to the heating. Small variations of this angle do not necessarily imply that the heating variations are also small. One nuance is that the measurements of changes in the magnetic field/flux are a combination of changes due to translational motions as well as variations in magnitude, so direct conversion into energy is not unambiguous. Nevertheless, the quiet Sun chromospheric and coronal heating requirements are $\sim 4 \times 10^6$ erg cm^{-2} s^{-1} and $\sim 3 \times 10^5$ erg cm^{-2} s^{-1}, respectively (Withbroe & Noyes 1977; Aschwanden 2004), suggesting that 10% changes in chromospheric output could be enough to sustain the quiet corona. The situation is more complex, however, in active region loops. Kano & Tsuneta (1996) and Katsukawa & Tsuneta (2005) quoted estimates of $\sim 10^6$ erg cm^{-2} s^{-1} for 'warm' loops and $\sim 10^7$ erg cm^{-2} s^{-1} for hot loops. This compares to $\sim 2 \times 10^7$ erg cm^{-2} s^{-1} for the chromosphere in active regions (Withbroe & Noyes 1977; Aschwanden 2004). Assuming that the strong basal levels of magnetic flux and Ca II emission in AR 10960 match this heating requirement, these numbers suggest that the 10–20% changes we observe on 'warm' EUV loop cooling time-scales of 20–30 mins could be enough to heat these loops impulsively at low frequency. These changes, and the 10–20% variations that occur over time-scales that are longer than a loop cooling time, would not be enough, however, to heat the hot loops.

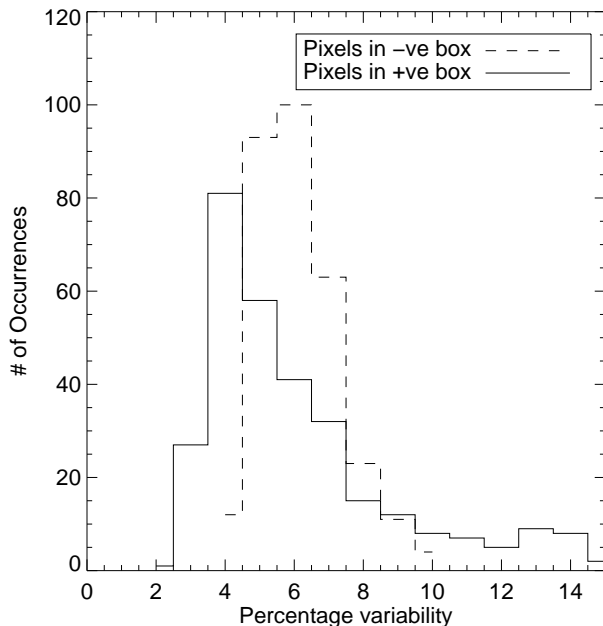Katsukawa & Tsuneta (2005) estimated the energy flux into

Fig. 19.— Distributions of Ca II intensity variability ($\sigma/\bar{I}$) expressed as percentages for the individual pixels within the same two moss boxes shown in Figure 18.

Fig. 20.— Distributions of Ca II intensity variability ($\sigma/\bar{I}$) and magnetic field variability ($\sigma/\bar{B}$) expressed as percentages for all the pixels in all the moss boxes shown in Figure 9.

coronal loops as a result of the dissipation of magnetic energy built up in coronal current sheets due to the braiding of the field by photospheric motions. They found that for a moss magnetic field strength measurement of 1.2kG, the heating requirement of hot loops (10^7 erg cm^{-2} s^{-1}) could be met. In their estimates, however, the energy flux is related to the magnetic flux as $F \propto B^2$, so that once again a 10–20% change in magnetic flux may meet the heating requirements of the 'warm' loops, but does not appear to supply enough energy to heat the hot loops. A definitive statement on this issue awaits more detailed theoretical modeling. These results suggest, however, that only the continuous input from the strong basal levels of magnetic flux and chromospheric emission, not the variations, appear to be enough to power the hot core loops rooted in the moss.

The results presented here, together with those in Paper 1 and Paper 2 and Antiochos et al. (2003), show a lack of variability in many types of diagnostic signatures: magnetic flux observations by SOT, coronal velocity measurements by EIS, EUV and X-ray intensities from *TRACE* and XRT, etc., and constitute a compelling body of evidence. Future instrumentation, however, may reveal all of these quasi-steady properties to be a distraction. It is possible, for example, that the magnetic field could appear steady in the lower atmosphere while it is braided in the corona and energy is released there. Heating by impulsive events could occur at coronal heights with no visible signature in the magnetic field at lower heights. The lack of variability in the EUV and X-ray data could indicate that the impulsive events occur on sub-resolution scales. Low frequency impulsive heating on unresolved scales could give the impression of high frequency (effectively steady) heating. These suggestions, of course, are difficult to test, since we do not know the spatial scale of the heating. Priest et al. (2002) suggest that the size scale of the fundamental kG flux tubes in the photosphere have diameters of 100km, and based on these arguments Klimchuk (2006) sug-
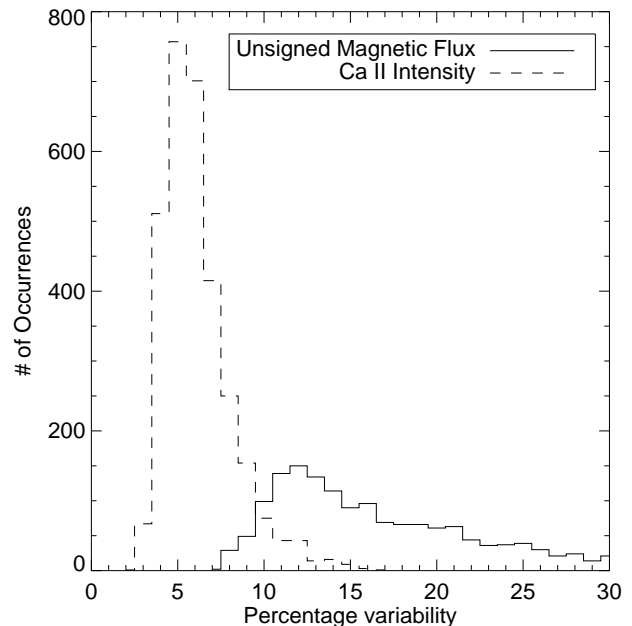
gests that a comparable spatial resolution may be able to resolve the strands making up the corresponding loops, though the current sheet interface may be smaller. We have shown here that the magnetic flux and chromospheric emission are quasi-steady on spatial scales approaching 100km. This is 4000 times smaller than studied by Antiochos et al. (2003) and should rule out models that predict low frequency impulsive heating on larger scales.

REFERENCES

Antiochos, S. K., Karpen, J. T., DeLuca, E. E., Golub, L., & Hamilton, P. 2003, ApJ, 590, 547

Antolin, P., Shibata, K., Kudoh, T., Shiota, D., & Brooks, D. 2008, ApJ, 688, 669

Aschwanden, M. J. 2004, Physics of the Solar Corona. An Introduction (Springer-Verlag)

Aschwanden, M. J., Nightingale, R. W., & Alexander, D. 2000, ApJ, 541, 1059

Aschwanden, M. J., Schrijver, C. J., & Alexander, D. 2001, ApJ, 550, 1036

Berger, T. E., de Pontieu, B., Fletcher, L., Schrijver, C. J., Tarbell, T. D., & Title, A. M. 1999a, Sol. Phys., 190, 409

Berger, T. E., de Pontieu, B., Schrijver, C. J., & Title, A. M. 1999b, ApJ, 519, L97

Brooks, D. H., et al. 2004, ApJ, 602, 1051

Brooks, D. H., Ugarte-Urra, I., & Warren, H. P. 2008, ApJ, 689, L77

Brooks, D. H., & Warren, H. P. 2009, ApJ, 703, L10

Brown, C. M., Feldman, U., Seely, J. F., Korendyke, C. M., & Hara, H. 2008, ApJS, 176, 511

Close, R. M., Parnell, C. E., Mackay, D. H., & Priest, E. R. 2003, Sol. Phys., 212, 251

Culhane, J. L., et al. 2007, Sol. Phys., 243, 19

de Pontieu, B., et al. 2007, PASJ, 59, 655

de Pontieu, B., Tarbell, T., & Erdélyi, R. 2003, ApJ, 590, 502

De Rosa, M. L., et al. 2009, ApJ, 696, 1780

Delaboudiniere, J.-P., et al. 1995, Sol. Phys., 162, 291

Dere, K. P., Landi, E., Mason, H. E., Monsignori Fossi, B. C., & Young, P. R. 1997, A&AS, 125, 149

Dere, K. P., Landi, E., Young, P. R., Del Zanna, G., Landini, M., & Mason, H. E. 2009, A&A, 498, 915

Domingo, V., Fleck, B., & Poland, A. I. 1995, Sol. Phys., 162, 1

Fletcher, L., & de Pontieu, B. 1999, ApJ, 520, L135

Handy, B. N., et al. 1999, Sol. Phys., 187, 229

Ichimoto, K., et al. 2008, Sol. Phys., 249, 233

Kano, R., & Tsuneta, S. 1996, PASJ, 48, 535

Katsukawa, Y., & Tsuneta, S. 2005, ApJ, 621, 498

Klimchuk, J. A. 2006, Sol. Phys., 234, 41

Korendyke, C. M., et al. 2006, Appl. Opt., 45, 8674

Kosugi, T., et al. 2007, Sol. Phys., 243, 3

Kubo, M., et al. 2007, PASJ, 59, 779

Lenz, D. D., Deluca, E. E., Golub, L., Rosner, R., & Bookbinder, J. A. 1999, ApJ, 517, L155

Lites, B., Casini, R., Garcia, J., & Socas-Navarro, H. 2007, Memorie della Societa Astronomica Italiana, 78, 148

Lundquist, L. L., Fisher, G. H., & McTiernan, J. M. 2008, ApJS, 179, 509

Mariska, J. T. 1987, ApJ, 319, 465

Mariska, J. T., Emslie, A. G., & Li, P. 1989, ApJ, 341, 1067

Martens, P. C. H., Kankelborg, C. C., & Berger, T. E. 2000, ApJ, 537, 471

Parker, E. N. 1988, ApJ, 330, 474

Patsourakos, S., & Klimchuk, J. A. 2008, ApJ, 689, 1406

Peter, H., & Judge, P. G. 1999, ApJ, 522, 1148

Porter, L. J., & Klimchuk, J. A. 1995, ApJ, 454, 499

Priest, E. R., Heyvaerts, J. F., & Title, A. M. 2002, ApJ, 576, 533

Sakamoto, Y., Tsuneta, S., & Vekstein, G. 2008, ApJ, 689, 1421

Scherrer, P. H., et al. 1995, Sol. Phys., 162, 129

Schrijver, C. J., Sandman, A. W., Aschwanden, M. J., & DeRosa, M. L. 2004, ApJ, 615, 512

Shimizu, T. 1995, PASJ, 47, 251

Suematsu, Y., et al. 2008, Sol. Phys., 249, 197

Title, A. 2009, in ASP CS 415: Hinode 2

Tripathi, D., Mason, H. E., Dwivedi, B. N., del Zanna, G., & Young, P. R. 2009, ApJ, 694, 1256

Tripathi, D., Mason, H. E., Young, P. R., & Del Zanna, G. 2008, A&A, 481, L53

Tsuneta, S., et al. 2008, Sol. Phys., 249, 167

Ugarte-Urra, I., Warren, H. P., & Brooks, D. H. 2009, ApJ, 695, 642

Vourlidas, A., Klimchuk, J. A., Korendyke, C. M., Tarbell, T. D., & Handy, B. N. 2001, ApJ, 563, 374

Warren, H. P., Ugarte-Urra, I., Brooks, D. H., Cirtain, J. W., Williams, D. R., & Hara, H. 2007, PASJ, 59, 675

Warren, H. P., Ugarte-Urra, I., Doschek, G. A., Brooks, D. H., & Williams, D. R. 2008a, ApJ, 686, L131

Warren, H. P., & Winebarger, A. R. 2006, ApJ, 645, 711

Warren, H. P., Winebarger, A. R., & Brooks, D. H. 2010, ApJ, 711, 228

Warren, H. P., Winebarger, A. R., & Hamilton, P. S. 2002, ApJ, 579, L41

Warren, H. P., Winebarger, A. R., Mariska, J. T., Doschek, G. A., & Hara, H. 2008b, ApJ, 677, 1395

Winebarger, A. R., Warren, H. P., & Mariska, J. T. 2003, ApJ, 587, 439

Winebarger, A. R., Warren, H. P., & Seaton, D. B. 2003, ApJ, 593, 1164

Withbroe, G. L., & Noyes, R. W. 1977, ARA&A, 15, 363

Young, P. R., Watanabe, T., Hara, H., & Mariska, J. T. 2009, A&A, 495, 587